processes

MDPI

Article

Flexible Ring Sensor Array and Machine Learning Model for the Early Blood Leakage Detection during Dialysis

Ping-Tzan Huang [1], Chia-Hung Lin [2,*] and Chien-Ming Li [3]

[1] Department of Maritime Information and Technology, National Kaohsiung University of Science and Technology, Kaohsiung City 80543, Taiwan
[2] Department of Electrical Engineering, National Chin-Yi University of Technology, Taichung City 41170, Taiwan
[3] Department of Infectious Disease, Chi Mei Medical Center, Tainan City 710033, Taiwan
* Correspondence: eechl53@gmail.com

Abstract: Severe blood leakage resulting from the detachment of dialysis tubing is often difficult to detect by nurses in busy clinics. This paper presents a flexible blood leakage detection system featuring a ring-light sensor array with an operating wavelength of 500–700 nm, which is held in place by the gauze covering the dialysis puncture site. A ring-light sensor is connected to a bidirectional hetero-associative memory network, which interprets detected changes in signal strength, the output signal of which is transmitted via WiFi to a server at the nursing station where a machine learning algorithm determines whether blood leakage has occurred. The compact design of this early warning system greatly enhances the comfort and mobility of patients undergoing dialysis. The efficacy of the proposed system was demonstrated in experiments involving artificial blood.

Keywords: hemodialysis; flexible ring sensor array; machine learning; bidirectional hetero-associative memory network; embedded system

check for updates

Citation: Huang, P.-T.; Lin, C.-H.; Li, C.-M. Flexible Ring Sensor Array and Machine Learning Model for the Early Blood Leakage Detection during Dialysis. *Processes* **2022**, *10*, 2197. https://doi.org/10.3390/pr10112197

Academic Editors: Blaž Likozar and Xiong Luo

Received: 18 September 2022
Accepted: 22 October 2022
Published: 26 October 2022

Publisher's Note: MDPI stays neutral with regard to jurisdictional claims in published maps and institutional affiliations.

Copyright: © 2022 by the authors. Licensee MDPI, Basel, Switzerland. This article is an open access article distributed under the terms and conditions of the Creative Commons Attribution (CC BY) license (https://creativecommons.org/licenses/by/4.0/).

1. Introduction

According to the 2020 annual report published by the US Renal Data System (USRDS) [1], Taiwan had the highest global prevalence of patients with end-stage renal disease undergoing dialysis as well as the highest annual incidence of new dialysis patients in 2018. In 2019, the number of dialysis patients in Taiwan exceeded 920,000, with an annual treatment cost of 53.3 billion NTD. Furthermore, the age of onset is gradually decreasing. These phenomena can largely be attributed to the long-term use the over-the-counter medicines, such as non-steroidal anti-inflammatory drugs, anticoagulants, and paracetamol to treat uremia. Dialysis can be categorized as hemodialysis (HD) and peritoneal dialysis (PD) [2]. At present, most dialysis patients in Taiwan undergo hemodialysis in medical centers, regional hospitals, or metropolitan hospitals three times per week for 3–4 h per session.

As shown in Figure 1a [3], hemodialysis machines are equipped with a roller pump to generate pressure for dialysate flow and generate a transmembrane pressure difference (approximately 250 mmHg) to facilitate the removal of blood from the body. One set of tubing carries uremic blood from the body to the hemodialysis machine, where an artificial kidney cleans the blood, after which another set of tubing returns the blood to the body. As shown in Figure 1b [4], arteriovenous shunts (AVSs) can be classified as an arteriovenous fistula (AVF) or arteriovenous graft (AVG) [4,5]. The safety of patients during dialysis treatment depends on the detection of blood leakage and the immediate notification of on-duty nursing staff. Existing hemodialysis machines monitor blood pressure, blood leakage, patient temperature, blood conductivity, blood PH, air bubble invasion, and the operating status of bypass devices [6,7].

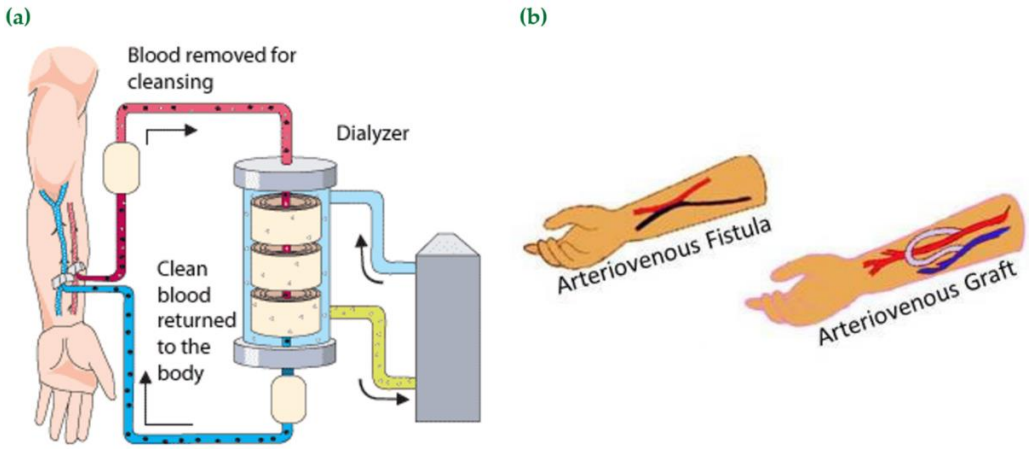


Figure 1. (**a**) Working principle of hemodialysis treatment and hemodialysis machine; (**b**) type of arteriovenous shunt (AVF and AVG).

Researchers have developed a number of schemes for the detection of blood leakage, including optical sensors, pad sensors, and wetness sensors. The blood detection system devised by Qing et al. [8] is based on non-volatile reagents. Nomura et al. [9] devised a short-circuit detection system based on electrodes patterned on cotton textiles using screen-offset printing technology. Shimazaki et al. [10] employed the evolution of color (chroma) in color sensors to detect blood leakage without the risk of malfunction due to chemical leakage or interference from obstacles along the light path. Tan et al. [11] detected blood leakage by examining changes in the intensity of LED light using principal components analysis (PCA). The three most common commercial devices used for the detection of blood leakage during dialysis include the Redsense® Monitor™ (Redsense® Medical Inc., Halmstad, Sweden, FDA-approved); HEMOdialert™ (Azacare Inc., Waikanae, New Zealand), and Leak Detector (Nipro Inc., Osaka, Japan) [12–14]. As shown in Figure 2a, the Redsense system uses a single-point near-infrared light in conjunction with a sensor held in place by the gauze covering the puncture site. Blood leaking into the gauze alters the signal received by the photo interrupter, signaling an alarm [12]. As shown in Figure 2b,c [13,14], the Azacare and Nipro devices are based on conductive circuits on water-absorbent materials, which short circuit when blood leakage occurs, sounding an alarm.

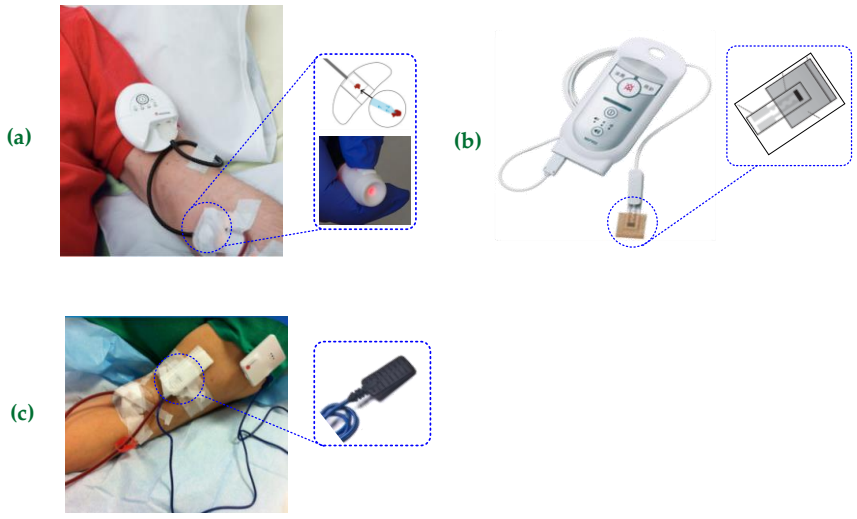


Figure 2. (**a**) Redsense® Monitor (light sensor); (**b**) HEMOdialert™ (moisture sensor); (**c**) Nipro moisture sensor.

The systems mentioned above include sensors, analog circuits, an alarm unit, and a wireless communication system within a bulky device worn on the arm or chest. In the event that blood leakage is detected during dialysis, the device transmits an alarm signal to the nursing station via Bluetooth. Note that these systems must be worn for an extended duration (3–4 h) and impose upon the patient undue stress by constraining their mobility. They can also hinder the operation of arteriovenous devices.

In the current study, we sought to combine the benefits of existing systems by creating a ring-light sensor array on a flexible printed circuit board (FPCB) [15–17] (see Figure 3). The light sensor is a semiconductor, the resistance of which decreases inversely with the intensity of the light striking it. Blood covering the light sensor can increase the photoresistance by several kiloohms (KΩ) or even megaohms (MΩ). A bleeder circuit and voltage follower transmit changes in voltage to an embedded computing unit, in which a bidirectional hetero-associative memory (BHAM) network machine learning model [18–20] determines the severity of the blood leakage. The portability of the unit was ensured by moving the alarm system to the nursing station to which an alarm is transmitted using a WiFi wireless network (IEEE 802.11 standard WLAN [21–23]). Experiments using artificial blood verified the efficacy of the proposed system.

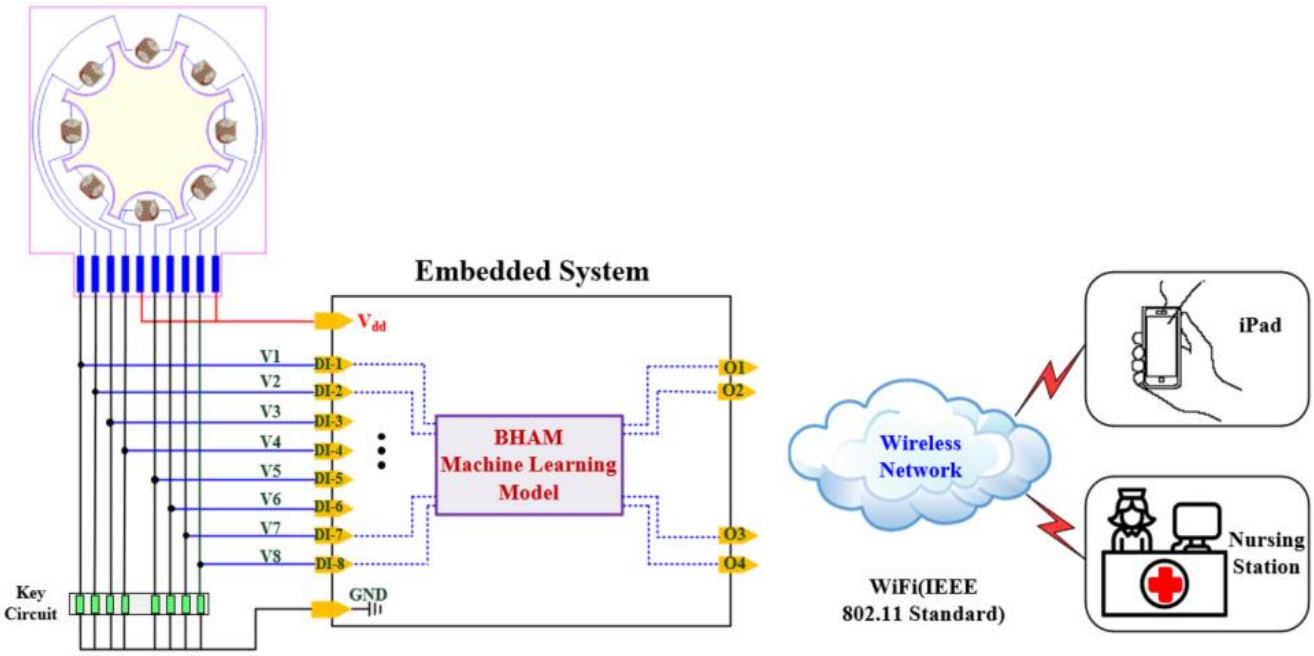


Figure 3. Structure of integrated flexible ring-light sensor array and machine learning model.

2. Materials and Methods

2.1. Flexible Ring-Light Sensor Array

High-sensitivity light sensors are widely used in electronic circuits. As shown in Figure 4a, most of these sensors are based on cadmium sulfide (CdS) or cadmium selenide (CdSe) [24], the resistance of which varies with light intensity, ranging from 300 Ω (at 1000 Lux) to 1 MΩ (at 0.1 Lux). In this study, eight light sensor elements were fabricated via digital cylinder printing in a ring formation on a thin, inexpensive flexible printed circuit board measuring 40 × 40 mm^2. This compact design allows placement within the gauze bandage at the puncture site. As shown in Figure 4b, uniform light distribution was ensured by creating a ring-light system comprising eight light sensors connected to a +5.0 VDC (current: 0.008–0.500 mA). Voltage signals from the eight light sensors (0 to 5.0 VDC) were sent to analog input ports, and mapping serial ports (MSPs) were connected to the key circuit resistor, which means that each DI port (DI-1 DI-8) was connected directly to a light sensor. This made it possible to apply a hard limit function on light sensor values expressed as

threshold values. Digital sensor signals (S_i; i = 1, 2, 3, . . . , 8) were converted into 8-bit binary patterns, as follows:

$$S_i = \begin{cases} 0, & if\ V_{cd} > V_i > V_{cd} \times 70\% \\ 1, & if\ V_i < V_{cd} \times 70\% \end{cases}, V_{cd} = +5.0 \quad (1)$$

where sensing state S_i = 1 indicates the logic state "High (1)" and S_i = 0 indicates logic state "(0)". Thus, sensor detection status can be derived from the 8-bit binary number as follows: $S = [s_1, s_2, s_3, s_4, s_5, s_6, s_7, s_8] = [0/1, 0/1, 0/1, 0/1, 0/1, 0/1, 0/1, 0/1]$. This generates 2^8 = 256 binary patterns corresponding to each $\boldsymbol{R}$ = [0/1, 0/1, 0/1, 0/1] pattern, as shown in Figure 5. Note that a value of "1" indicates the detection of an anomaly at that point, whereas a value of "0" indicates no anomaly. For example, an output pattern of $\boldsymbol{R}$ = [0 0 0 0] would indicate risk level 1 (normal state), whereas $\boldsymbol{R}$ = [0 1 0 0] would indicate risk level 2 (mild blood leakage), $\boldsymbol{R}$ = [0 0 1 0] would indicate risk level 3 (moderate blood leakage), and $\boldsymbol{R}$ = [0 0 0 1] would indicate risk level 4 (serious blood leakage). Hence, the combinations generated by the four risks level were as follows:

- Risk level 1: 0 sensors detected (normal)
- Risk level 2: $\leqq$3 sensors detected (Nr = 91 combinations)
- Risk level 3: $\leqq$6 sensors detected (Nr = 153 combinations)
- Risk level 4: $\leqq$7 sensors detected (Nr = 9 combinations)

where $\boldsymbol{R}$ indicates the level of risk. We then used these data as inputs for a BHAM machine learning model to estimate the severity of blood leakage based on the corresponding 256 binary models.

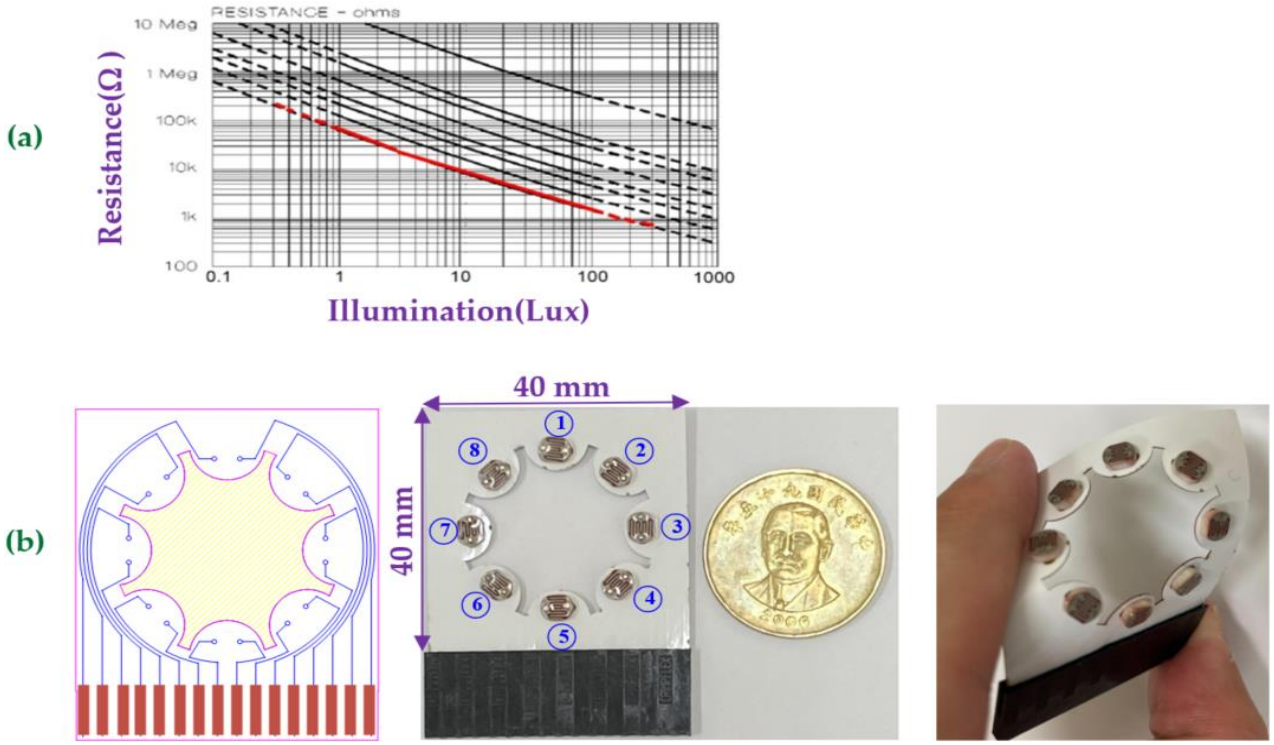


Figure 4. (**a**) Correlation curve showing resistance (Ω) as a function of light intensity (Lux) as measured using the light sensor (log-log). (**b**) Flexible ring-light sensor array.

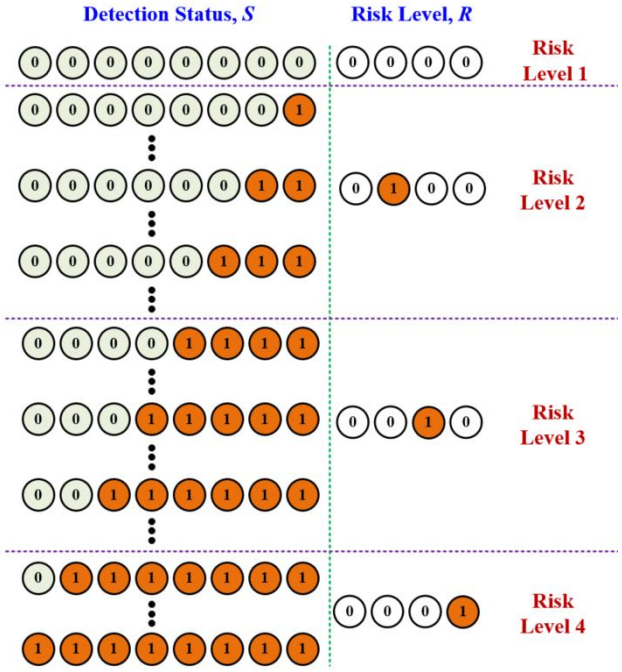


Figure 5. Correspondence between different combinations of binary patterns and risk levels.

2.2. Bidirectional Hetero-Associative Memory Machine Learning Model

Associative memory machine learning methods can be classified as auto-associative and hetero-associative (BHAM). The latter employs a feedback mechanism, which allows the synthesis of new model patterns and noise filters [18–20]. The network includes an input layer, an output layer, and a network connection layer. This type of model saves high-dimensional training models in the connection and correlation matrix and then uses human cognition to construct a model. The weights applied to input data are encoded in the weighting matrix based on various conditions. By reducing the 256 groups of input–output matched training data for each patient, the BHAM model resolves the problem of non-linear identification.

However, in the processing of binary and bipolar data, auto-associative and hetero-associative memory machine learning algorithms can also be used to store information and matrices using noise-free versions of input mode X and output mode Y. Thus, non-linear separable tasks can be performed simply by altering the configuration of the linear processing unit and Gaussian function, as shown in Figure 6.

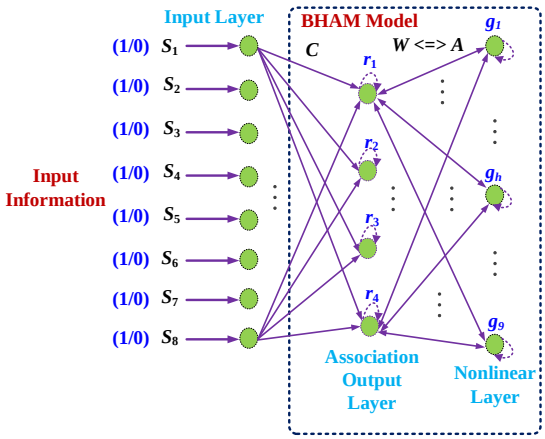


Figure 6. Proposed bidirectional hetero-associative memory network model.

In the current study, the BHAM machine learning model was implemented in two stages: a learning stage and a bidirectional association stage:

- Learning stage:

Step (1) This involved the construction of training input–output correspondence patterns $\underline{S}_k$ and $\underline{R}_k$, where the input pattern was $\underline{S}_k$, k = 1, 2, 3, . . . , 256, the connection status vector was $\underline{S}_k = [s_{k1}, \ldots, s_{ki}, \ldots, s_{kn}]^t$, n = 8, and the risk pattern vector was $\underline{R}_k = [r_{k1}, \ldots, r_{ki}, \ldots, r_{km}]^t$, m = 4.

Step (2) This involved using K pairs of training modes to construct connection matrix $\boldsymbol{C}$:

$$C = \sum_{k=1}^{K} \underline{R}_k \underline{S}_k^t \tag{2}$$

where the dimensionality of matrix $\boldsymbol{C}$ was $[c_{ij}]n \times m$. Thus, the dimension corresponding to the input–output model can be converted from $K \times n$ and $K \times m$ into $n \times m$.

Step (3) The eigenvalue of connection matrix $\boldsymbol{C}$ was calculated as follows:

$$\lambda_j = \frac{1}{n} \sum_{i=1}^{n} c_{ij}, \quad j = 1, 2, 3, \ldots, m \tag{3}$$

Thus, in the current study, n = 8 indicates an 8-input binary system and m = 4 indicates four risk levels. The relationship between weight matrix $\boldsymbol{W}$ and correlation matrix $\boldsymbol{A}$ is described using Equation (4), as follows:

$$W = \begin{bmatrix} \theta_0 \times \lambda_1 & \theta_1 \times \lambda_1 & \cdots & \theta_5 \times \lambda_1 & \cdots & \theta_7 \times \lambda_1 & \cdots \\ \theta_0 \times \lambda_2 & \theta_1 \times \lambda_2 & \cdots & \theta_5 \times \lambda_2 & \cdots & \theta_7 \times \lambda_2 & \cdots \\ \theta_0 \times \lambda_3 & \theta_1 \times \lambda_3 & \cdots & \theta_5 \times \lambda_3 & \cdots & \theta_7 \times \lambda_3 & \cdots \\ \theta_0 \times \lambda_4 & \theta_1 \times \lambda_4 & \cdots & \theta_5 \times \lambda_4 & \cdots & \theta_7 \times \lambda_4 & \cdots \end{bmatrix} \Leftrightarrow A = \begin{bmatrix} 1 & 0 & \cdots & 0 & \cdots & 0 & \cdots \\ 0 & 1 & \cdots & 0 & \cdots & 0 & \cdots \\ 0 & 0 & \cdots & 1 & \cdots & 0 & \cdots \\ 0 & 0 & \cdots & 0 & \cdots & 1 & \cdots \end{bmatrix} \tag{4}$$

where $\theta_h = h$, h = 0, 1, 2, . . . , 8 indicate the weights corresponding to the risk levels, and correlation matrix A indicates the binary value of the coded risk level associated with those weights.

- Bidirectional association stage:

Step (1) The storage element is used to obtain connection matrix $\boldsymbol{C}$, correlation matrix $\boldsymbol{A}$, and weight matrix $\boldsymbol{W}$. The voltage of the flexible ring array sensor is converted into a binary value (0/1) using Equation (1), and the test input pattern $\underline{S}^0 = [s_1, \ldots, s_5, \ldots, s_8]^t$ is applied to the connection network.

Step (2) This is the association stage, which involves calculating the output pattern $\underline{R}^0 = [r_1, r_2, r_3, r_4]^t$ using Equations (5) and (6):

$$\underline{R}^0 = C\underline{S}^0 \tag{5}$$

$$r_j^0 = \sum_{i=1}^{9} c_{ij} s_j^0, \quad j = 1, 2, 3, 4 \tag{6}$$

Step (3) The pattern from the output unit is sent to the non-linear layer (association unit) for analysis using Equations (7) and (8):

$$D_h = \|\underline{w_h} - \underline{R^0}\| = \sqrt{\sum_{i=1}^{9} \left(w_{hj} - r_j^0\right)^2} \tag{7}$$

$$g_h = \exp\left(\frac{1}{2\sigma^2} \times (D_h)^2\right), \quad h = 1, 2, 3, \cdots, 9 \tag{8}$$

where σ is the standard variable, $\underline{w_h}$ is the i^{th} column in the weight matrix, $\underline{G}^0 = [g_1, g_2, g_3, g_4, \ldots, g_9]$, D_h indicates the estimated distance, and g_h is the output Gaussian function used primarily to assess the degree of similarity between output mode $\underline{R}^0$ and weight vector wh. The value varied between 0 and 1, where $g_h \longrightarrow 0$, indicates low correlation and $g_h \longrightarrow 1$ indicates high correlation.

Step (4) Transmit the outputs of g_h units to the r_j^0 unit with nonlinear feedback with a hard limit function (threshold value of 0.5). A new output r_j^1 unit pattern can then be derived using Equations (9)–(11), as follows:

$$v_j = \sum_{h=1}^{9} a_{jh} g_h, \quad j = 1, 2, 3, 4 \tag{9}$$

$$r_j^1 = \begin{cases} 1, & v_j \geq 0.50 \\ 0, & v_j < 0.50' \end{cases} \tag{10}$$

$$\underline{R}^1 = \left[r_1^1, r_2^1, r_3^1, r_4^1 \right] \tag{11}$$

Step (5) A lack of change in output unit pattern $\underline{R}^1$ and output unit pattern $\underline{R_{max}}$ is taken as an indication of bidirectional stability, such that bidirectional association is immediately halted. Otherwise, the program returns to Step 2 until the following bidirectional termination conditions are met:

$$\underline{R_{\max}} = \operatorname{argmax}\left(r_j^1 \right) \geq 0.50 \tag{12}$$

The design of the ring-light sensor array and BHAM model proposed in this study was easily implemented in an embedded system (ES) that included a Wifi wireless communication system (WLAN; 2.4 GHz) for the transmission of alerts to the nursing station or portable computing device within an interior space of up to 20 × 30 m^2.

3. Results and Discussions

3.1. Experiment Setup

The analog blood leak detection equipment and BHAM were implemented using a National Instruments™ myRIO-1900 (Austin, TX, USA) [25]. Data collection coding, basic mathematical operations, and formulaic operations were implemented using the MathScript encoder (National Instruments™ LabVIEW, Austin, TX, USA). Data transmission was implemented using WiFi (IEEE 802.11 Standards, Wireless Local Area Network). The human–machine interface used to display the results (sensor data acquisition system, risk level warning, and other information) was designed using the graphical program encoder provided in NI™ LabVIEW. An analog mapping serial port (MSP) embedded in the system received voltage values from the eight sensor nodes in the ring-light sensor array. The eight light sensor voltage values (V1 to V8) were used to derive the voltage of the eight light sensors in the ring array by Equation (1). When in the normal state, the logic "0", the threshold was $V_{cd} > V_i > V_{cd} \times 70\%$, i = 1, 2, 3, … ,8. Similarly, the blood leak state, the logic "1", the threshold was $V_i < V_{cd} \times 70\%$. Artificial blood (2–10 mL) was used to simulate blood in the experiment and the reaction time of the sensor was between 1 and 10 s.

3.2. Preliminary Detection Tests

A total of 256 combinations of input and output training modes were used in the construction of two matrices for use, a set of binary patterns. Weight matrix $\boldsymbol{W}$ and correlation matrix $\boldsymbol{A}$ were constructed using Equation (4) as follows:

$$W \Leftrightarrow A$$
$$\begin{bmatrix} 0 & 29\times 0 & 90\times 0 & 9\times 0 \\ 0 & 29\times 1 & 90\times 1 & 9\times 1 \\ 0 & 29\times 2 & 90\times 2 & 9\times 2 \\ 0 & 29\times 3 & 90\times 3 & 9\times 3 \\ 0 & 29\times 4 & 90\times 4 & 9\times 4 \\ 0 & 29\times 5 & 90\times 5 & 9\times 5 \\ 0 & 29\times 6 & 90\times 6 & 9\times 6 \\ 0 & 29\times 7 & 90\times 7 & 9\times 7 \\ 0 & 29\times 8 & 90\times 8 & 9\times 8 \end{bmatrix} \Leftrightarrow \begin{bmatrix} 1 & 0 & 0 & 0 \\ 0 & 1 & 0 & 0 \\ 0 & 1 & 0 & 0 \\ 0 & 1 & 0 & 0 \\ 0 & 0 & 1 & 0 \\ 0 & 0 & 1 & 0 \\ 0 & 0 & 1 & 0 \\ 0 & 0 & 0 & 1 \\ 0 & 0 & 0 & 1 \end{bmatrix}$$

As shown in Figure 6, the BHAM machine learning model had eight input nodes, four output nodes, and nine non-linear processing nodes (Gaussian function). Below, we present an example instance of blood leakage (>10 mL of artificial blood) covering sensors #1, #2, #3, and #4. The process of measurement and calculation is outlined in the following:

Step (1) The processing of blood leakage detection values V = [V_1, V_2, V_3, V_4, V_5, V_6, V_7, V_8]^t = [3.39, 3.30, 3.17, 3.23, 4.28, 4.20, 4.18, 4.23]^t resulted in the following output: $\underline{S}^0$ = [1, 1, 1, 1, 0, 0, 0, 0]^t, based on the hard limit function.

Step (2) $\underline{R}^0$ = [0, 0, 0, 0]t was applied to input mode $\underline{S}^0$, whereupon Equations (5) and (6) were used to obtain the correlation output model $\underline{R}^0$.

Step (3) After converting output model $\underline{R}^0$ into a Gaussian function, Equations (7) and (8) were respectively used to calculate the output vector $\underline{G}^0$ and distance D_h, as follows:

$$\underline{G}^0 = [0.000, 0.000, 0.000, 0.002, 0.838, 0.003, 0.000, 0.000]^t;$$

$$D = [381.649, 286.667, 191.687, 96.716, 2.828, 93.306, 188.276, 283.256, 378.238]^t.$$

where g_5 indicated the maximum value in $\underline{G}^0$ and (argmin $\|D_5\|$ = 2.828) had the highest similarity in measurement categories. Thus, the risk level corresponding to these values was 3.

Step (4) From the Gaussian function, we obtained a new output v_j unit for which we calculated the following: [v_1, v_2, v_3, v_4,]^t = [0.000, 0.002, 0.840, 0.000]^t, which was then used to derive v_j = [0, 0, 1, 0]^t using the hard limit function.

Step (5) When bidirectional stability was achieved, the sensor calculations were terminated and the human–machine interface presented an alarm indicating risk level 3, as shown in Figure 7.

The simulation of different light sensors was covered with artificial blood (2–10 mL) for the mean of ten experimental results, as shown in Table 1. When the ring-light sensors were in a normal state, the voltage from each of the eight sensors averaged 4.15–4.30 volts, such that the sensing state was S = [0, 0, 0, 0, 0, 0, 0, 0]. When two of the light sensors were occluded by artificial blood, the light sensor voltage range decreased to 3.1–3.48 volts with a sensing state of S = [0, 0, 0, 0, 0, 0, 1, 1]. When four or seven of the light sensors were occluded, the light sensor voltage range varied between 3.1–3.48 V for a sensing state of S = [0, 0, 0, 0, 1, 1, 1, 1] or S = [0, 1, 1, 1, 1, 1, 1, 1], respectively.

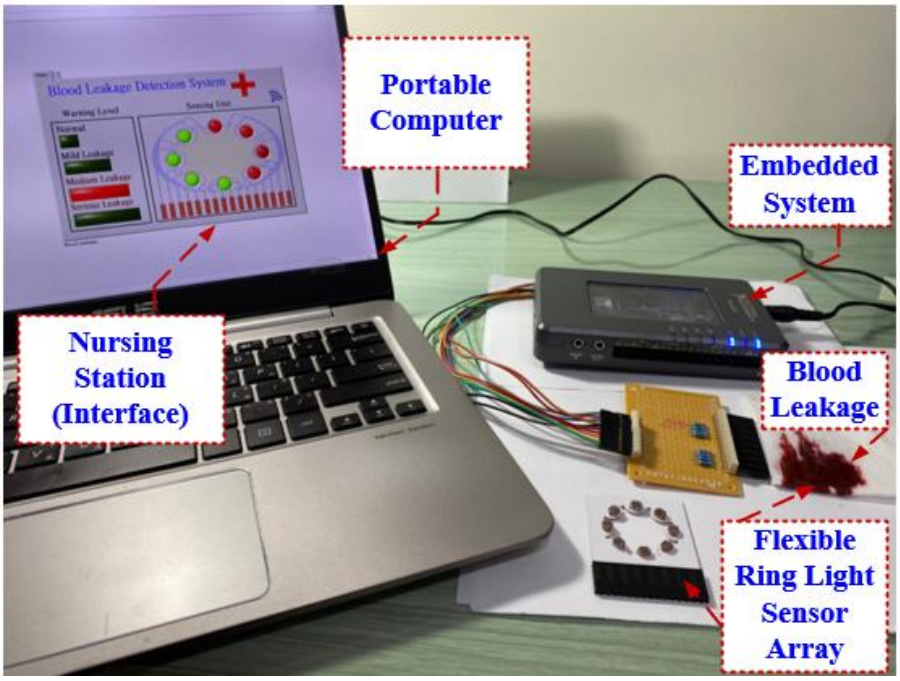


Figure 7. Experiment setup and sensor array detection results.

Table 1. Mean results of 10 experiments using artificial blood (2–10 mL).

Sensor Point / Event	Level 1: Normal Voltage (V) and S	Level 2 Voltage (V) and S	Level 3 Voltage (V) and S	Level 4 Voltage (V) and S
1	4.15–4.30, 0	3.1–3.48, 1	3.1–3.48, 1	3.1–3.48, 1
2	4.15–4.30, 0	3.1–3.48, 1	3.1–3.48, 1	3.1–3.48, 1
3	4.15–4.30, 0	4.15–4.30, 0	3.1–3.48, 1	3.1–3.48, 1
4	4.15–4.30, 0	4.15–4.30, 0	3.1–3.48, 1	3.1–3.48, 1
5	4.15–4.30, 0	4.15–4.30, 0	4.15–4.30, 0	3.1–3.48, 1
6	4.15–4.30, 0	4.15–4.30, 0	4.15–4.30, 0	3.1–3.48, 1
7	4.15–4.30, 0	4.15–4.30, 0	4.15–4.30, 0	3.1–3.48, 1
8	4.15–4.30, 0	4.15–4.30, 0	4.15–4.30, 0	4.15–4.30, 0

3.3. Performance Comparisons

Table 2 presents a performance comparison of the current system and previous works [17]. The proposed BHAM model used matrix calculations in the learning stage without iterative updating of the network model. This made it possible to reduce the dimensionality of the training model, internal memory requirements, and computation time. The 8-4-9 network model and Euler distance method were used to measure the degree of similarity between weight patterns in weight matrix $\boldsymbol{W}$. Argument $\|D_h\|$ (h = 1, 2, 3, . . . , 9) is a free parameter used mainly to configure the standard deviation of the Gaussian function in the recall stage. This parameter has a self-regulatory function that adjusts non-linear functions to deal with non-linear separation problems. In the recall stage, the hetero-associative memory process required $\leq$2 iterations, thereby eliminating any need to adjust network parameters. Furthermore, only 416 bytes of storage space was required. The mean execution duration to achieve bidirectional stability and determine blood leak risk level was <0.15 ms. We achieved a hit rate of 100% in simulations involving 256 events. We employed the current injection method and Jacobi and Gauss–Seidel methods to solve the linear equation, whereas an iterative calculation process (2 < iterations < 25) was used to obtain the voltages of nodes in the analog sensor. Using node voltage to identify instances of artificial blood leakage required 512 bytes of memory.

Table 2. Performance comparison of bidirectional hetero-associative memory network and virtual self-organizing direct current grid model.

Task \ Methods	Bidirectional Hetero-Associative Memory Network (BHAM)	Virtual Self-Organizing DC Grid Model [17]
Network Architecture	(8-4-9)	-
Memory Storage	*C* Matrix (4 × 8): 128 bytes *W* Matrix (4 × 9): 144 bytes *A* Matrix (4 × 9): 144 bytes	n^2 for matrix Y and 3 × *n* for vectors, *I*, *V*(*p*), *V*(*p* + 1) 520 bytes
Training Data	Connecting Matrices *C*, *W*, and *A* 256 input–output pairs of training patterns	-
Process Unit	Gaussian Function Hard Limit Function	Multiplication, Division, and Subtraction
Algorithm	Bidirectional Associative Memory	Current Injection Method and Jacobi and Gauss–Seidel Method (<25 iterative computations)
Learning Stage	Matrix Operation	-
Recalling Stage	Iteration computation ≤ 2	-
Execution Time	Average Time: <0.15 ms	Average Time: <0.30 ms
Accuracy	100%	100%

3.4. Proposed System Versus Similar Sensing Devices in the Literature

Table 3 compares the blood detection system proposed in this paper to comparable works in the literature. Daniel et al. [8] proposed a gas-based method capable of detecting the presence of blood within 30 s; however, having the alarm unit and battery attached to the arm is somewhat uncomfortable for the patient. Nomura et al. [9] devised a short-circuit detection system based on electrodes patterned on cotton textiles using screen-offset printing. Note however that the authors did not provide detailed data analysis pertaining to the performance of their scheme. Shimazaki et al. [10] proposed the use of LED color sensors to detect blood leakage; however, their system requires an external battery. Tan et al. [11] also used LED light intensity to detect blood leakage, but with the alarm unit and battery attached to the arm. Lee et al. [26] used deep learning to determine whether the data from LED sensors were indications of blood leakage; however, the success rate of their system was only 83.7%. Chuang et al. [27] used a photo-interrupt sensor attached to the patient's arm to detect instances of blood leakage, after which a digital signal is sent to the nursing station via Bluetooth 4.0, triggering an alarm within 1.6 s after the initial detection. The system proposed by Zeng et al. [28] used two photodiode sensors to detect blood leakage and send the resulting digital signal via WiFi to a microcontroller computing unit (MCU) to determine whether to issue an alarm. Nonetheless, detection is performed at intervals of 5 s. Note that most of the research above focused on the sensor, sensing direction, power supply support, or alarm unit on the arm. Only two papers [9,27] refer to detection sensitivity (15 µL and 0.01 mL, respectively).

The system developed in this study sought to eliminate the disadvantages of previous systems while retaining the advantages. The proposed system was evaluated using artificial blood to simulate leakage events, and the results indicate the mean of 10 experiments, as shown in Table 1. The proposed detection unit was sensitive to the leakage of only 2 mL and the total detection time was <0.15 ms. The transmission of information to the nurse station via WiFi eliminates the need to attach an alarm unit to the patient's arm and the embedded supply power ensures that signals are not interrupted by power outages.

The proposed system employs a flexible light-array sensor within a compact lightweight housing to ensure the comfort and mobility of the patient during hemodialysis.

Table 3. Comparison of current work with previous systems in the literature.

Design Items / Literature	Sensor	Sensing Direction	Algorithm	Sensitivity	Detector Time	Connect to Nurse Station	Battery Support	The Alarm Unit Set up on the Arm
[8]	Gas detector	One sensor	-	-	<30 s	WiFi Wireless	Yes	Yes
[9]	Wetness sensing	Multi sensors	-	15 μL	-	-	-	-
[10]	LED color sensors	One sensor	Light intensity	-	-	-	Yes	No
[11]	LED light sensor	One sensor	Light intensity	-	-	No	Yes	Yes
[26]	LED light sensor	One sensor	-	-	-	WiFi Wireless	Yes	Yes
[27]	Photo interrupter	One sensor	Analog	0.01 mL	1.6 s	Bluetooth 4.0	Yes	Yes
[28]	Photodiode	Two sensors	Digital	-	Every 5 s	WiFi Wireless	Yes	No
This Work	Light sensors	Flexible ring array	Digital	2 mL	<0.15 ms	WiFi Wireless	No	No

4. Conclusions

This paper presents a preliminary assessment of a flexible ring-light sensor array implemented in conjunction with BHAM to identify instances of blood leakage during hemodialysis. Unlike IR light sensors, the proposed photocell sensor is thin, light, flexible, inexpensive, and easily implemented as a wearable device. The sensor based on a ring-light array also enables multi-directional sensing to enhance system robustness. Analog signals indicating a change in sensor voltage are converted into a digital signal, which is input into an algorithm tasked with assessing the level of risk. The BHAM model is simple to configure and quick to train. The training and internal memory storage requirements are lower than those of conventional machine learning methods. By minimizing computation, the proposed system also enables rapid detection. In experiments using artificial blood, the hit rate was 100% and the sensor demonstrated good sensitivity using blood samples as small as 2 mL. The entire unit complies with IEC 60601-1 Part 1–11: 2015 standards for electromagnetic compatibility [29,30], including the design, circuit performance, and risk assessment methods.

Author Contributions: Conceptualization, P.-T.H., C.-H.L. and C.-M.L.; analysis and materials, P.-T.H. and C.-H.L.; data analysis, P.-T.H. and C.-H.L.; writing—original draft preparation, P.-T.H., C.-H.L. and C.-M.L.; writing—review and editing, P.-T.H. and C.-H.L.; supervision, P.-T.H., C.-H.L. and C.-M.L.; funding acquisition, P.-T.H. and C.-H.L. All authors have read and agreed to the published version of the manuscript.

Funding: This work was supported by the Ministry of Science and Technology, Taiwan, under contract number: MOST 111-2222-E-992-004, duration: 1 August 2022–31 July 2023.

Institutional Review Board Statement: Not applicable.

Informed Consent Statement: Not applicable.

Data Availability Statement: Not applicable.

Conflicts of Interest: The authors declare that they have no conflict of interest.

Abbreviations

USRDS	US Renal Data System
HD	Hemodialysis
PD	Peritoneal dialysis
AVSs	Arteriovenous shunts
AVF	Arteriovenous fistula
AVG	Arteriovenous graft
PCA	Principal Components Analysis
FPCB	Flexible printed circuit boards
KΩ	kilo-ohms
MΩ	megaohms
BHAM	Bidirectional hetero-associative memory
CdS	Cadmium sulfide
CdSe	Cadmium selenide
MSPs	Mapping serial ports
ES	Embedded system
MCU	Microcontroller

References

1. 2020 Annual Data Report. Available online: https://adr.usrds.org/2020/ (accessed on 20 October 2022).
2. Hemodialysis. Available online: https://www.lucenxia.com.my/types-of-peritoneal-dialysis (accessed on 20 October 2022).
3. All About Dialysis. Available online: https://www.idcantalya.com/en/dialysis/ (accessed on 20 October 2022).
4. Leo, K.M. Haemodialysis Access. Available online: https://www.vascular.com.hk/page37.php (accessed on 20 October 2022).
5. Allon, M.; Robbin, M.L. Increasing arteriovenous fistulas in hemodialysis patients: Problems and solutions. *Kidney Int.* **2002**, *62*, 1109–1124. [CrossRef] [PubMed]
6. Murdeshwar, H.N.; Anjum, F. Hemodialysis. 2020. Available online: https://europepmc.org/article/NBK/nbk563296 (accessed on 20 October 2022).
7. Azar, A.T.; Canaud, B. Hemodialysis system. In *Modelling and Control of Dialysis Systems*; Springer: Berlin/Heidelberg, Germany, 2013; pp. 99–166.
8. Engvall, D.; Stroemsten, P. Detection of blood leakage by detecting a volatile agent. U.S. Patent No. 9,492,091, 15 November 2016.
9. Nomura, K.I.; Horii, Y.; Kanazawa, S.; Kusaka, Y.; Ushijima, H. Fabrication of a textile-based wearable blood leakage sensor using screen-offset printing. *Sensors* **2018**, *18*, 240. [CrossRef] [PubMed]
10. Shimazaki, T.; Kawakubo, Y.; Hara, S.; Hitosugi, T.; Yokoyama, T.; Miki, Y. Blood Leakage Determination Using the Chromaticity of a Color Sensor. *Adv. Biomed. Eng.* **2019**, *8*, 177–184. [CrossRef]
11. Tan, C.-H.; Khaw, J.-Y.; Wong, Y.-C.; Chionh, C.-Y.; Foong, S. BWatch: A Non-invasive Blood Leakage Detection Device using Robust Reflectance-based Sensing. In Proceedings of the 2019 IEEE International Conference on Cybernetics and Intelligent Systems and IEEE Conference on Robotics, Automation and Mechatronics, Bangkok, Thailand, 18–20 November 2019; pp. 350–355.
12. Redsensemedical Venous Needle Dislodgement. Available online: https://redsensemedical.com/ (accessed on 20 October 2022).
13. Hemodialerttm. 2005. Available online: https://www.hemodialert.com/hemodialert-hemodialysis-alarm.php (accessed on 16 October 2022).
14. NIPRO. 2014. Available online: https://www.nipro.co.jp/ (accessed on 20 October 2022).
15. Gao, W.; Emaminejad, S.; Nyein, H.Y.Y.; Challa, S.; Chen, K.; Peck, A.; Fahad, H.M.; Ota, H.; Shiraki, H.; Kiriya, D.; et al. Fully integrated wearable sensor arrays for multiplexed in situ perspiration analysis. *Nature* **2016**, *529*, 509–514. [CrossRef] [PubMed]
16. Lin, C.-H.; Chen, W.-L.; Li, C.-M.; Wu, M.-J.; Huang, P.-T.; Chen, Y.-S. Assistive technology using integrated flexible sensor and virtual alarm unit for blood leakage detection during dialysis therapy. *Healthc. Technol. Lett.* **2016**, *3*, 290–296. [CrossRef] [PubMed]
17. Huang, P.-T.; Jong, T.-L.; Li, C.-M.; Chen, W.-L.; Lin, C.-H. Integrating flexible sensor and virtual self-organizing DC grid model with cloud computing for blood leakage detection during hemodialysis. *IEEE Trans. Biomed. Circuits Syst.* **2017**, *11*, 784–793. [CrossRef] [PubMed]
18. Berberian, N.; Aamir, Z.; Hélie, S.; Chartier, S. Encoding sparse features in a bidirectional associative memory. In Proceedings of the 2016 International Joint Conference on Neural Networks (IJCNN), Vancouver, BC, Canada, 24–29 July 2016; pp. 5119–5126.
19. Lin, C.-H.; Chen, W.-L.; Kan, C.-D. Inflow and outflow stenoses screening on biophysical experimental arteriovenous graft using big spectral data and bidirectional associative memory machine learning model. *IET Cyber-Phys. Syst. Theory Appl.* **2019**, *4*, 139–147. [CrossRef]
20. Chartier, S.; Giguère, G.; Langlois, D. A new bidirectional heteroassociative memory encompassing correlational, competitive and topological properties. *Neural Netw.* **2009**, *22*, 568–578. [CrossRef] [PubMed]

21. *IEC 60601-1-11:2015*; Medical Electrical Equipment-Part 1–11: General Requirements for Basic Safety and Essential Performance-Collateral Standard: Requirements for Medical Electrical Equipment and Medical Electrical Systems Used in the Home Healthcare Environment. International Electrotechnical Commission: London, UK, 2015.
22. *IEEE Std 802.11™*; Institute of Electrical and Electronics Engineers et. al. IEEE Computer Society: Part 11: Wireless LAN Medium Access Control (MAC) and Physical Layer (PHY) Specifications. The Institute of Electrical and Electronics Engineers: Piscataway, NJ, USA, 2012; pp. 1–2793.
23. Vallozzi, L.; Van Torre, P.; Hertleer, C.; Rogier, H.; Moeneclaey, M.; Verhaevert, J. Wireless communication for firefighters using dual-polarized textile antennas integrated in their garment. *IEEE Trans. Antennas Propag.* **2010**, *58*, 1357–1368. [CrossRef]
24. Ada, L. Cds Cells, Photoresistors, & Light Dependent Resistors (ldr). 2012. Available online: https://learn.adafruit.com/photocells/measuring-light (accessed on 20 October 2022).
25. Doering, E. *NI myRIO Project Essentials Guide*; National Technology and Science Press: Austin, TX, USA, 2014; pp. 165–168.
26. Lee, H.-C.; Lin, J.-S. An Open-Source Wearable Sensor System for Detecting Extravasation of Intravenous Infusion. *IEEE Trans. Instrum. Meas.* **2020**, *70*, 1–11. [CrossRef]
27. Chuang, H.-C.; Shih, C.-Y.; Chou, C.-H.; Huang, J.-T.; Wu, C.-J. The development of a blood leakage monitoring system for the applications in hemodialysis therapy. *IEEE Sens. J.* **2015**, *15*, 1515–1522. [CrossRef]
28. Zeng, J.-H.; Tsai, Y.-S. A Wireless Hemodialysis Blood Oozing Detection and Alarm System. In *International Conference on the Development of Biomedical Engineering in Vietnam*; Springer: Singapore, 2018; pp. 441–444.
29. IEC 60601-1 International Standard, Medical Electrical Equipment–Part 1: General Requirements for Basic Safety and Essential Performance. Available online: https://www.iso.org/standard/41986.html (accessed on 20 October 2022).
30. IEC PAS 63023:2016. Medical Electrical System Input Interface for Haemodialysis Equipment for Use of External Alarming Device. Available online: https://webstore.iec.ch/publication/24041 (accessed on 20 October 2022).